

Angular Dependence of \mathcal{K} -Distributed Sonar Data

Gilles Le Chenadec, Jean-Marc Boucher, *Member, IEEE*, and Xavier Lurton

Abstract—Backscattered signal statistics are widely used for target detection and seafloor characterization. The \mathcal{K} -distribution shows interesting properties for describing experimental backscattered intensity statistics. In addition to the fact that its probability distribution function accurately fits actual sonar data, it advantageously provides a physical interpretation linked to the backscattering phenomenon. Sonar systems usually record backscattered signals from a wide angular range across the ship's track. In this context, previous studies have shown that backscatter statistics strongly depend on the incidence angle. In this paper, we propose an extension of previous works to model the angular evolution of the \mathcal{K} -distribution shape parameter. This evolution is made clear and analyzed from experimental data recorded with two sonar systems: a 95-kHz multibeam echosounder and a 110-kHz sidescan sonar. Model fitting with data backscattered from six seafloor configurations shows the improvement provided by our extension as compared to two previous models.

Index Terms—Seafloor classification, sonar statistical analysis, \mathcal{K} -distribution.

I. INTRODUCTION

ACTIVE high-frequency sonar systems have been widely used to study statistical features of acoustical signals backscattered by the seafloor. Interest in describing and modeling such statistical distributions has increased with the development of high-resolution sonars. Such systems are designed to increase detection performance and to improve the signal-to-noise ratio within the resolution cell or the instantaneous insonified area. Consequently, echo-amplitude distributions are characterized by heavy tails whose shape may be different from the traditional Rayleigh model. Beyond target-detection purposes, backscattered signals are studied to extract clues useful for seafloor classification and characterization. In this context, an appropriate modeling of backscattered signal statistics may provide a useful link to geoacoustic parameters of the seafloor.

The classical Rayleigh distribution is applicable to backscattered amplitudes when the deterministic number of scatterers N_s within the resolution cell is large enough so that the central limit theorem is valid and the distribution of scatterers has no influence. Non-Rayleigh distributions appear when the central limit theorem hypotheses are not verified [1]. This can be due to a high variance of the number of scatterers, or scatterers characterized by nonidentically distributed random variables.

Available statistical models highlight the main role of N_s depending on both the sonar geometry and the seafloor properties.

Statistical analysis of backscattered amplitude or intensity typically consists in fitting a set of theoretical distributions in order to determine which one describes measurements the best [2]–[5]. Some physical models connect empirical densities to geoacoustic parameters [6]. Models by Crowther [7], Middleton [8], or MacDaniel [9] belong to this category but are difficult to use. Based on Jakeman's works on the \mathcal{K} -distribution, two other physical models take into account the system characteristics and a geoacoustic representation of the seafloor. First, Lyons and Abraham [5], [10] suggest new physical interpretations leading to a backscattered intensity distributed according to a \mathcal{K} -distribution. They show the link between the number of scatterers or sediment patches inside the resolution cell, the shape parameter of the \mathcal{K} -distribution, and the system characteristics. Second, Oliver [11] includes correlation effects between scatterers and the finite size of the resolution cell to derive statistical moments of the backscattered intensity, distributed according to a correlated \mathcal{K} -distribution. Applied to either sonar or radar data, Oliver's works have shown good ability to model empirical statistics. Oliver's model (OM) has been applied by Hellequin *et al.* to multibeam-echosounder data [12] and extended to take into account the evolution of the distribution according to the incidence angle, a characteristic feature of sonar data; this is made possible by accounting for the local bathymetry. Although this model showed possibilities for modeling angular dependence of the shape parameter, this approach remains unsatisfactory in some respects. A major drawback is the fact that the model cannot account for the diversity of seabed backscattered responses; its development is based on an oversimplified backscattering strength model. Moreover, the model has not been fitted to a sufficient variety of different seabeds.

In this paper, an extension of the model developed by Hellequin *et al.* is proposed. Section II presents the model principles. In Section III, the angular dependence of backscattered intensity is first studied on measurements recorded from two sonar systems operating in the same frequency range but with a different geometry. Three models of backscattered intensity are then fitted with the experimental data recorded with the multibeam system. Section IV sets out conclusions.

II. MODEL OF BACKSCATTERED-INTENSITY STATISTICS

OM [11] for the backscattered intensity is based on a scattering point approach. First, the surface is modeled by a dense network of scatterers described individually by their amplitudes a_n and phases ϕ_n . Second, the complex field \mathcal{Z} is the incoherent sum of the contributions of the scatterers N_s inside

Manuscript received March 14, 2006; revised October 10, 2006.

G. Le Chenadec and J.-M. Boucher are with GET, École Nationale Supérieure des Télécommunications, Bretagne, CS83818, 29238 Brest Cedex 3, France (e-mail: Le.Chenadec@free.fr; JM.Boucher@enst-bretagne.fr).

X. Lurton is with the Institut Français de Recherche pour l'Exploitation de la Mer, 29280 Plouzané, France (e-mail: Xavier.Lurton@ifremer.fr).

Color versions of one or more of the figures in this paper are available online at <http://ieeexplore.ieee.org>.

Digital Object Identifier 10.1109/TGRS.2006.888454

the resolution cell. The number of scatterers N_s is assumed deterministic and proportional to the size of the resolution cell. Furthermore, their positions are random inside this insonified area. Thus

$$\mathcal{Z} = \sum_{n=1}^{N_s} a_n \exp(i\phi_n). \quad (1)$$

The backscattered intensity is split into

$$I \equiv |\mathcal{Z}|^2 = R \cdot S \quad (2)$$

combining two different physical processes: The underlying-scene reflectivity R (assumed Γ -distributed, see [13]) depending on the physical properties of the surface elementary scatterers and the speckle phenomenon, which is the consequence of the random distribution of these scatterers within the resolution cell. Moreover, S is classically assumed noncorrelated, independent of R , and exponentially distributed [14].

Under the previous assumptions about R and S models, the backscattered intensity is \mathcal{K} -distributed [15]

$$f_I(I) = \frac{2}{\Gamma(\nu_I)\Gamma(L)} \left(\frac{L\nu_I}{\mu_I}\right)^{\frac{L+\nu_I}{2}} I^{\frac{L+\nu_I-2}{2}} \times K_{\nu_I-L} \left[2\sqrt{\frac{L\nu_I I}{\mu_I}} \right] \quad (3)$$

where μ_I is the scale parameter, ν_I the shape parameter, K_{ν_I-L} is the modified Bessel function of the second kind, and L is the multilook parameter. As μ_I is estimated by the backscattered-intensity mean, it is related to the classical backscattering strength.

The model proposed by Oliver [11] is based on two assumptions. First, the correlation of scatterers depends on the surface model described by the assumed stationary random variable R , distributed according to the Γ -distribution $f_R(R)$ and by the spatial correlation coefficient ρ_R

$$f_R(R) = \left(\frac{\nu_R}{\mathbb{E}[R]}\right)^{\nu_R} \frac{R^{\nu_R-1}}{\Gamma(\nu_R)} \exp\left(-\frac{\nu_R R}{\mathbb{E}[R]}\right) \quad (4)$$

$$\begin{aligned} \rho_R(\xi) &= \frac{\mathbb{E}[R(\xi_1)R(\xi_2)] - \mathbb{E}[R]^2}{\mathbb{E}[R]^2 - \mathbb{E}[R]^2} \\ &= \nu_R \left(\frac{\mathbb{E}[R(\xi_1)R(\xi_2)]}{\mathbb{E}[R]^2} - 1 \right) \end{aligned} \quad (5)$$

where $\xi = |\xi_1 - \xi_2|$ is the distance between scatterers at spatial coordinates $\xi_1 = (x_1, y_1)$ and $\xi_2 = (x_2, y_2)$, ν_R is a shape parameter of the Γ -distribution, and $\mathbb{E}[\cdot]$ is the statistical expectation. The correlation functions are usually 1-D or 2-D exponential-like or Gaussian-like. In this paper, a 2-D-Gaussian correlation function has been used

$$\rho_R(x, y) = \exp\left(-\frac{x^2}{Lc_t^2}\right) \cdot \exp\left(-\frac{y^2}{Lc_l^2}\right) \quad (6)$$

where $\xi = (x, y)$, $x = x_1 - x_2$, $y = y_1 - y_2$, and (Lc_t, Lc_l) are the correlation lengths in both across-track and along-track directions.

Second, the wave-scattering process in OM takes into account characteristics of the sonar system. The backscattered intensity $I(\xi)$ at location ξ from a scene with complex scattering amplitude $A(\xi)$ (linked by $R = |A(\xi)|^2$) is given by [11]

$$\begin{aligned} I(\xi) &\equiv |\mathcal{Z}(\xi)|^2 \\ &= \int_{\mathbb{R}^2} [A(\xi_1)A^*(\xi_2)h(\xi - \xi_1)h^*(\xi - \xi_2)] \times d\xi_1 d\xi_2 \end{aligned} \quad (7)$$

where $*$ indicates the complex conjugation, \mathcal{Z} is the complex backscattered field, and h is point-spread function of the sonar (footprint of the emitted signal on the bottom).

In the case of a sonar system, the function h can be approximated by

$$h(x_1, x_2) = \begin{cases} \frac{1}{L a_t \cdot L a_l}, & \text{if } -\frac{L a_t}{2} \leq x_1 \leq \frac{L a_t}{2} \\ & \text{and } -\frac{L a_l}{2} \leq x_2 \leq \frac{L a_l}{2} \\ 0, & \text{otherwise} \end{cases} \quad (8)$$

where $L a_t$ and $L a_l$ are the resolution-cell lengths, respectively, in the across-track and along-track directions.

An interesting property is given by Oliver [14]

$$\begin{aligned} \mathbb{E}[I(\xi)] &= \int_{\mathbb{R}} [\mathbb{E}[|A(\xi)|^2] |h(\xi - \xi_1)|^2] d\xi_1 \\ &= \mathbb{E}[R(\xi)]. \end{aligned} \quad (9)$$

In [16], Oliver derived the second-order normalized moments of intensity for a roughness characterized by a Gaussian correlation function (6)

$$\frac{\mathbb{E}[I^2]}{\mathbb{E}[I]^2} = \frac{L+1}{L} \left[1 + \frac{F_{\text{Gauss}}(\gamma_t)F_{\text{Gauss}}(\gamma_l)}{\nu_R} \right] \quad (10)$$

where

$$\begin{aligned} F_{\text{Gauss}}(x) &= \frac{\sqrt{\pi}}{x} \cdot \text{erf}(x) + \frac{\exp(-x^2)}{x^2} - x^{-2} \\ \gamma_t &= \frac{L a_t}{L c_t} \\ \gamma_l &= \frac{L a_l}{L c_l} \end{aligned} \quad (11)$$

and $\text{erf}(\cdot)$ is the error function.

Starting from Oliver's work, Hellequin *et al.* proposed a new model [12] introducing the combined effects of the randomness of incidence angles and the angular evolution of the backscattering strength. For sonar system data, the backscattering strength presents an angular dependence characterized by strong energy variations at specular and grazing incidences. In addition, the estimate of incidence angles on the bottom presents a random character due to bathymetry measurement uncertainties. These assumptions lead to a shape of the R -distribution, dependent on the incidence angle.

The incidence angle of the backscattered signal is computed by $\theta_{\text{inc}} = \theta_{\text{emi}} - \phi_{\text{bat}}$, where θ_{emi} is the emission angle and ϕ_{bat} is the bottom-slope angle (Fig. 1). The uncertainty of

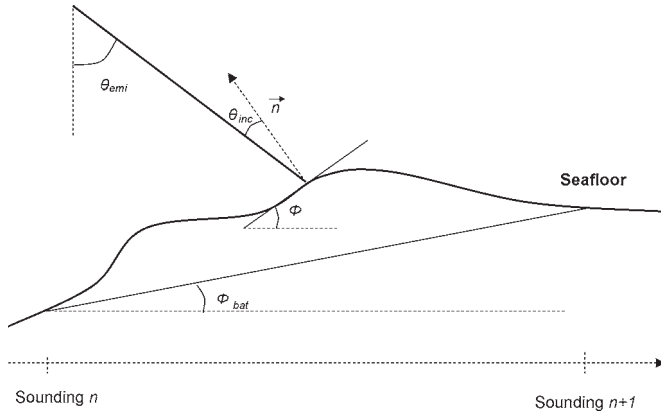


Fig. 1. Backscatter incidence angle of a sample is $\theta_{\text{inc}} = \theta_{\text{emi}} - \phi$. Due to the resolution of bathymetric data, it is estimated by $\theta_{\text{inc}} = \theta_{\text{emi}} - \phi_{\text{bat}}$.

bathymetric data randomizes local slopes ϕ_{bat} and, consequently, incident angles θ_{inc} . In [12], the model assumes a Gaussian distribution for local slopes, centered on zero and with standard deviation σ . The distribution of the new random variable θ_{inc} is then Gaussian ($\mathcal{N}(\theta_{\text{emi}}, \sigma^2)$)

$$f_{\phi_{\text{bat}}}(\phi) = \frac{1}{\sqrt{2\pi}\sigma} \exp\left(-\frac{\phi^2}{2\sigma^2}\right)$$

$$\Rightarrow f_{\theta_{\text{inc}}}(\phi) = \frac{1}{\sqrt{2\pi}\sigma} \exp\left(-\frac{(\theta_{\text{emi}} - \phi)^2}{2\sigma^2}\right). \quad (12)$$

In addition, taking into account the product model (2) and the independence of the random variables R and S , one gets the property (9)

$$\mathbb{E}[I] = \mathbb{E}[R] = \mathbb{E}[\text{BS}(\theta_{\text{inc}})]. \quad (13)$$

The backscattering angular model used in [12] is a simplified model combining a Gaussian law for specular angles and a Lambert law for grazing angles

$$\text{BS}(\theta_{\text{inc}}) = A \exp(-\alpha\theta_{\text{inc}}^2) + B \cos^\beta(\theta_{\text{inc}}) \quad (14)$$

making it possible to derive the m -order moments of R

$$\mathbb{E}[R^m] = \int_{\mathbb{R}} \text{BS}^m(\theta_{\text{inc}}) f_{\theta_{\text{inc}}}(\theta_{\text{inc}}) d\theta. \quad (15)$$

But, the model retained by Hellequin *et al.* for backscattering strength does not describe the whole range of seabed-backscattering angular behaviors. A β -Lambert model for the grazing angles [changing the $\cos^2(\theta_{\text{inc}})$ term by $\cos^\beta(\theta_{\text{inc}})$] in (14) appears to be better justified in comparison with actual backscattering strength measurements [17]. In this paper, we investigate this assumption extending the model proposed by Hellequin *et al.* Unfortunately, the derivation of the R moments (15) cannot be achieved analytically. The variable ϕ_{bat} describing local slopes centered on zero, an extension consists in approximating the $\cos^\beta(\theta_{\text{emi}} - \phi)$ function by a series expansion.

Approximating with a third-order series expansion in ϕ around zero, (14) becomes

$$\begin{aligned} \text{BS}(\theta_{\text{inc}}) &= A \exp(-\alpha\theta_{\text{inc}}^2) + B \cos^\beta(\theta_{\text{inc}}) \\ &= A \cdot \exp(-\alpha(\theta_{\text{emi}} - \phi)^2) + (b_1 + b_2\phi + b_3\phi^2 + b_4\phi^3) \end{aligned} \quad (16)$$

where

$$\begin{cases} b_1 = B \cdot \cos^\beta(\theta_{\text{emi}}) \\ b_2 = B \cdot \beta \cdot \cos^{\beta-1}(\theta_{\text{emi}}) \cdot \sin(\theta_{\text{emi}}) \\ b_3 = \frac{b_1 \cdot \beta}{2} [(\beta - 1) \cdot \tan^2(\theta_{\text{emi}}) - 1] \\ b_4 = \frac{b_2 \cdot \beta}{6} [(\beta^2 - 3\beta + 2)(1 + \tan^2(\theta_{\text{emi}})) - \beta^2]. \end{cases} \quad (17)$$

The two first moments become

$$\mathbb{E}[R] = C_1 \cdot \exp(-D_1\theta_{\text{emi}}^2) + b_1 + b_3 \cdot \sigma^2 \quad (18)$$

$$\mathbb{E}[R^2] = J_1 + J_2 + J_3 \quad (19)$$

where

$$\begin{cases} C_1 = \frac{A}{\sqrt{1+2\alpha\sigma^2}} & D_1 = \frac{\alpha}{1+2\alpha\sigma^2} \\ C_2 = \frac{A^2}{\sqrt{1+4\alpha\sigma^2}} & D_2 = \frac{2\alpha}{1+4\alpha\sigma^2} \\ C_3 = \frac{\sigma^2}{1+2\alpha\sigma^2} \end{cases} \quad (20)$$

and

$$\begin{cases} J_1 = C_2 \cdot \exp(-D_2\theta_{\text{emi}}^2) \\ J_2 = b_1^2 + (b_2^2 + 2b_1b_3)\sigma^2 + 3(b_3^2 + 2b_2b_4)\sigma^4 + 15b_4^2\sigma^6 \\ J_3 = 2C_1 \cdot \exp(-D_1\theta_{\text{emi}}^2) \\ \quad \times (b_1 + b_3C_3 + 6b_4C_3^2 + 2\alpha b_2C_3\theta_{\text{emi}} \\ \quad + 4\alpha^2C_3^2b_3\theta_{\text{emi}}^2 + 8\alpha^3C_3^3b_4\theta_{\text{emi}}^3). \end{cases} \quad (21)$$

Finally, since the variable R is assumed Γ -distributed, the following property allows to determine ν_R :

$$\frac{\text{Var}[R]}{\mathbb{E}[R]^2} = \frac{1}{\nu_R}. \quad (22)$$

The shape parameter of the \mathcal{K} -distribution of I can be obtained through the shape parameter of the Γ -distribution and sonar recording characteristics

$$\nu_I = \frac{\nu_R}{F_{\text{Gauss}}(\gamma_t) F_{\text{Gauss}}(\gamma_l)}. \quad (23)$$

The normalized differences between Hellequin's model (ADK) and our approach (by taking $\beta = 2$) have been displayed in Fig. 2 according to incidence angles, for variations of σ . The errors due to the approximation of the series expansion are not significant (about 0.02), validating in that sense our approach.

III. SONAR-DATA STUDY

In this section, the experimental setup used for at-sea measurements is first described. Characteristic angular evolutions for six seafloor configurations are set out. Finally, we confront our model with measurements and quantitatively compare results to OMs and ADKs.

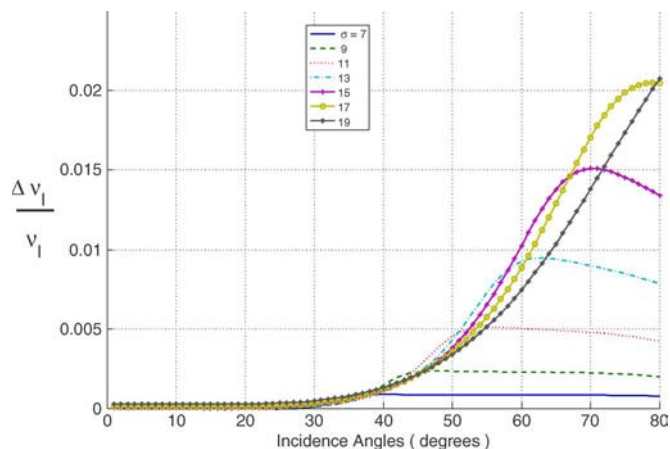


Fig. 2. Normalized difference between ADK and EADK models for calculation of ν_I and for different values of σ .

A. Experimental Setup

The data used in this study were recorded during a cruise conducted by IFREMER in the Baie de Douarnenez (France). Sonar signals were recorded from shallow water sites (from 10–40 m) corresponding to various geological facies. Data sets recorded under well-controlled conditions were intended for technical research tasks in sedimentary acoustics and processing of bathymetry imagery. Furthermore, a systematic comparison was to be carried out between two sonar system measurements: multibeam echosounder and sidescan sonar, operating in the same frequency range but with a different geometry.

The multibeam Simrad EM1000 provides both backscattering strength imagery and bathymetry. This echosounder emits a windowed sinusoidal signal of central frequency of 95 kHz, duration of 0.2 ms, and emitted level of 224 dB (ref 1 μ Pa at 1 m). In its shallow-water mode, 60 3.3° -wide beams are formed over an angular sector of 150° . The data correction process (whose detailed description may be found in [12] and [18]) has been applied to our data in order to obtain calibrated seafloor backscattering strength measurements. Processing artifacts are first removed: the time-varying-gain (TVG law) parameters as given by the manufacturer are compensated for, in order to retrieve the actual echo level; the in-water propagation losses and instantaneous signal footprint area are estimated and compensated in order to obtain the intrinsic backscattering strength of the local seafloor. Regarding the effects of array directivity small fluctuations, the correction method is based on the identification of the individual beam directivity patterns directly on the experimentally recorded backscattered amplitudes (see [18]), finally, allowing to correct each backscattering value for the beam set. Finally, bathymetric data recorded by the multibeam system give access to the local seafloor slopes and make it possible to improve the estimated angle dependence of the measured backscatter. This methodology has proven to give good valuable results [18], the major limitation being for the low-incidence (typically $[-15^\circ, 15^\circ]$) angle sector, where the intricate time-angle interdependence in a highly unstable backscatter context makes it very difficult to get a proper angle dependence.

The Edgetech DF1000 sidescan sonar works at two nominal frequencies of 112 and 384 kHz; in this paper, only the lower frequency data have been examined (actually two slightly different frequencies are used on port and starboard sides of the sonar, leading to different directivity patterns). Limited analysis elements were provided by the manufacturer (TVGs law, receiver sensitivity, nominal working values of transmit levels, beam apertures, and signal duration), but were found to be actually insufficient for a thorough analysis of the data. Hence, a series of calibration measurements had to be performed in IFREMER's test tank, leading to a more accurate knowledge of the sonar parameters. The directivity patterns in both directions were carefully measured and tabulated for further compensation processing. The emitted signal has a nominal duration of 0.1 ms, but is actually imperfectly stable due to the signal generation technology used in this particular sonar type. Since, in a classical side-scan sonar context, no direct measurement of angle is available and the time-angle relation is not as well-defined as in multibeam echosounders since a dedicated process had to be defined [17], encompassing the retrieval of acquisition geometry (especially incidence angles), a description of this method is given in the Appendix. The final inversion of the sonar equation including array patterns, propagation loss corrections, area normalization, and slope correction is based on the same principles as for the multibeam echosounder.

During the investigation of sidescan sonar data, it was found that wrong recording-parameter settings had corrupted the data. The time series received by the system are decimated: among three samples, the maximum is selected. This process makes irrelevant the quantitative comparison between sonar system statistics. Hence, the shape parameter of the \mathcal{K} -distribution values will not be quantitatively analyzed for this sonar; only the evolution of the angular dependence will be qualitatively compared with the multibeam echosounder data angular evolution. However, a new estimate of the shape parameter (based on the estimation of the statistical moments of the maximum sample distribution) has been created to compensate the effect of the decimation.

B. Seafloor Acoustical Measurements

Four areas were selected for their sedimentary homogeneity. Geological information was obtained from grab samples, and relief features from video sequences and multibeam bathymetry. These four sites are described below, and grab samples are displayed in Fig. 3:

- 1) Site 5 is located by the central point [$48^\circ 18.5' \text{ N} - 4^\circ 23' \text{ W}$]. Covered with *fine sand*, this bottom is sedimentary homogeneous and presents a very light downward bathymetry from north–northeast to south–southwest (0.4%). The video records show a microroughness characterized by centimetric ripples over a sandy seafloor, which does not seem significantly orientated.
- 2) The central point of site 2 is located at coordinates [$48^\circ 10.2' \text{ N}, 4^\circ 29.55' \text{ W}$]. This seafloor is also made up of *fine sand*. Bathymetry features a light downward slope (0.7%) from northwest to southeast. This bottom is



Fig. 3. From up to down, grab samples and inwater snapshot of sites 5, 2, 4, and 3.

sedimentary identical to site 5 and presents the same type of centimetric microrelief.

- 3) Site 4 is a *coarse-sand* sediment, located at the position [48° 08.35' N, 4° 25.9' W]. The main particularity of this seabed is its roughness showing current ripples, in which one can observe a significant proportion of shell fragments. The mean ripple wavelength was estimated at 1.2 m directly on sidescan sonar images, and the mean direction of the crest lines is north-south.
- 4) Site 3 is a *mixture of sand and mud* with a flat bathymetry. Its central point is located at the position [48° 08.622' N, 4° 20.859' W]. Microripples were detected on the video records without particular orientation.

Two data sets have been added to extend the seafloor variety to heterogeneous ones. The first one, Site 1, is a muddy interface colonized by a bivalve population, and the second one, Site 6, features rock outcrops.

TABLE I
NONREJECTION RATE OVER THE RANGE OF AVAILABLE ANGULAR SECTORS FOR THE MULTIBEAM ECHOSOUNDER

Site	Rayleigh	2-comp Rayleigh	3-comp Rayleigh
Mud+Bivalve (1)	23.1	96.1	100
Fine Sand (2)	3.9	62.3	100
Muddy Sand (3)	82.7	97.3	100
Coarse Sand (4)	27.5	98.6	100
Fine Sand (5)	14.5	73.7	80.3
Rock outcrops(6)	18.2	56.8	90.9
Site	K	Weibull	Log-Normal
Mud+Bivalve (1)	97.4	96.2	5.19
Fine Sand (2)	72.6	32.9	2.63
Muddy Sand (3)	94.7	93.3	5.3
Coarse Sand (4)	92.8	73.4	7.6
Fine Sand (5)	79.7	42.8	3.95
Rock Outcrops(6)	89.1	47.7	6.8

The backscatter statistical analysis requires independent and identically distributed samples. To ensure independence, samples contained in an individual ping have been decimated [10]. To analyze the statistical distribution characteristics independently of the effects of angular variations of backscatter, the data for each incidence angle have been normalized so that the intensity is set to unity. To ensure that the normalized and independent samples are identically distributed, the Spearman correlation coefficient test and the Mann-Whitney test (also called the Wilcoxon test [19]) have been applied. Most of the data passed the tests for a degree of confidence of 95%; samples that failed have been removed from the analysis.

The data has been binned by the angular sector in the range $[-75^\circ, 75^\circ]$ for the multibeam echosounder ($[-85^\circ, 85^\circ]$ for the sidescan sonar). The bins are located on positions equally spaced on seafloor across the ship's track.

Each seafloor data set has been incoherently averaged to reduce speckle leading to an across-track resolution of 1 m. Afterward, the number of samples used for each set is between 500 and 1000.

Several distributions (K -model, Rayleigh, mixtures of Rayleigh, Weibull, and Log-normal) have been compared to provide the best model for these experimental data on the full range of angles. To evaluate the capacity and the precision of these statistical models, the Kolmogorov-Smirnov (KS) test [20] has been used to compare the empirical data with the candidate distributions with a 5% significance level.

The results for the multibeam echosounder data are presented in terms of success rate (according to the KS-statistics) on the available range in Table I.

The Rayleigh distribution does not accurately model experimental data (Table I): success rates of this theoretical model are mostly low. The Log-normal model is particularly unsuited for these data: rates presented in the table show that even for the very heterogeneous and/or rough seafloors, the model does not provide correct fits. Among the four other models, two are two-parameter distributions (Weibull and K). The last two are the Rayleigh mixtures with two components (four parameters) and with three components (six parameters). Each mixture distribution presents a mixture rate parameter and a scale parameter providing a model for sedimentary mixtures. Rates for

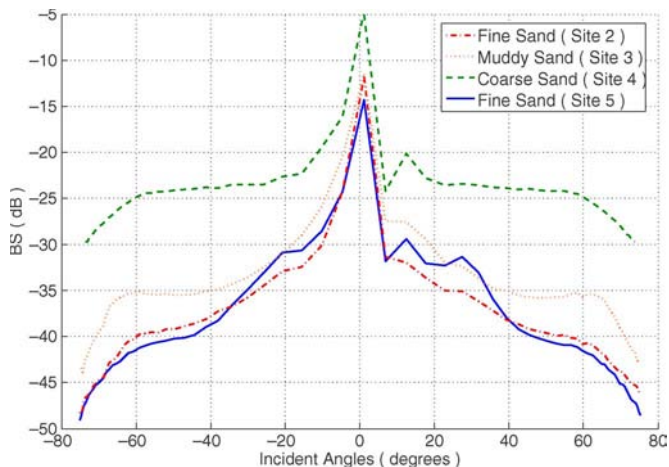


Fig. 4. Angular evolution of the mean μ_I (in decibels) for multibeam echosounder data and soft sediments.

these four distributions are the most significant (Table I). The Rayleigh mixture models and the \mathcal{K} -distributions are the most robust models in the data fit observed on the available angular range. The former show an undeniable robustness to model data and could be used in sonar image segmentation applications based on an algorithm whose decision is based on the maximum likelihood. However, our choice to model the backscattering statistics is the \mathcal{K} -distribution whose fits are mostly successful and has the advantage to present a compromise between a reduced number of parameters; the benefit of its physical interpretation and its goodness-of-fit.

Then, the angular evolution of backscattering statistics via the evolution of one parameter of the \mathcal{K} -distribution has been investigated. As mentioned previously, the scale parameter μ_I is the average backscattering strength, and its analysis is not carried out in this paper. Rather, the shape parameter is studied in order to complete the seafloor-characterization potential of the backscattering strength. Its estimate is based on the first and second statistical moment of intensity [21].

C. Measurements Analysis

Figs. 4–7 display angular evolutions of both parameters of the \mathcal{K} -distribution (3), in the case of multibeam-echosounder data for six seafloor configurations. Note that the parameter μ_I has been estimated before normalization (see the previous section) and is displayed for information purposes in decibels (hence, equivalent to the backscattering strength mean level).

Results for the μ_I angular evolution show a rich variety of behaviors for backscatter intensity. First, a global dynamic greater than 15 dB is found at midgrazing angles, making clear the variety of sediment properties analyzed in this data set. The behavior according to the angle is quite classical at first sight, with a global decreasing trend for low grazing angles. Note that the high-intensity contrast observed between the specular peak and the oblique values (up to 15–20 dB, even for rough-seafloor interfaces) may be beyond what is typically expected at such a frequency (95 kHz). Moreover, μ_I curves for small positive angles show a little peak. This may be related to imperfections in

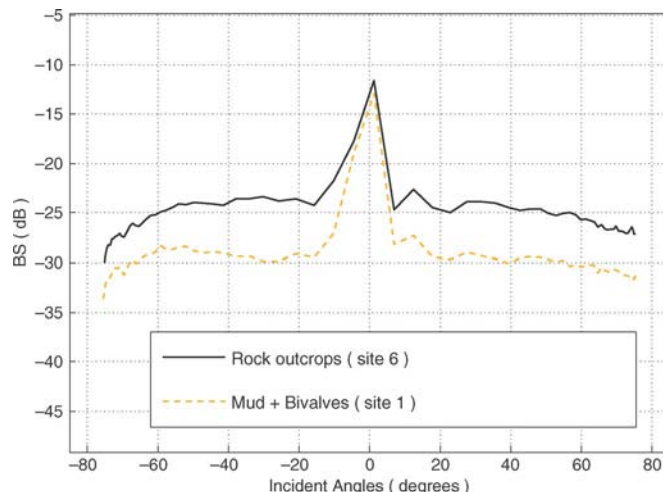


Fig. 5. Angular evolution of the mean μ_I (in decibels) for multibeam echosounder data and rough sediments.

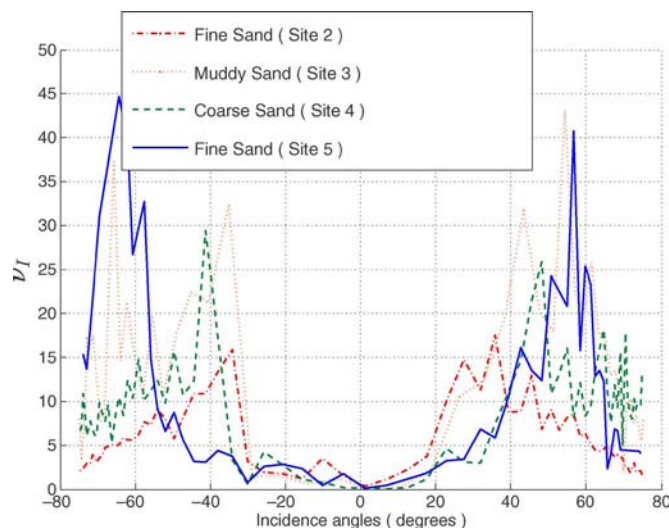


Fig. 6. Angular evolution of the shape ν_I for multibeam echosounder data and soft sediments.

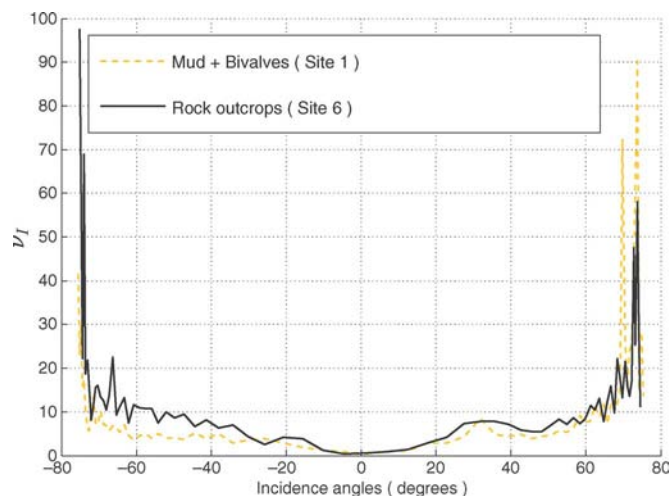


Fig. 7. Angular evolution of the shape ν_I for multibeam echosounder data and rough sediments.

the data-compensation processing in the specular-angle range, where the physical phenomena are especially complex [12].

The angular evolution of the shape parameter may be split into three sectors (Figs. 6 and 7). For angles close to the vertical ($|\theta| < 20^\circ$), the shape parameter, with very small values, does not discriminate between seabed types. These low values indicate strong heterogeneity. For intermediate angles between specular and grazing, rough-sediment curves (Fig. 7) have a softer slope than for smoother sediments (Fig. 6). At grazing angles, a characteristic inversion of slope is observable in Fig. 6 contrary to plots of Fig. 7 whose curves show monotonous slopes.

Two phenomena may explain the angular evolution of backscattered statistics and, in particular, the shape parameter. On the one hand, sonar characteristics (array geometry and signal duration) determine the size of the resolution cell and, hence, the number of scatterers within the resolution cell. On the other hand, backscatter mechanisms between acoustical waves and rough seafloor are angular dependent. The variations angular of the backscattering strength are well known, and results of this paper show the angular dependence of backscatter statistical parameters.

For steeper incidence angles, the shape-parameter values are very low, indicating a strong heterogeneity. Signal fluctuations, especially high in this sector due to the quick angular variations of the backscattering strength, are responsible for these low values despite the large extent of the resolution cell.

For intermediate angles, the global increase is due to the extension of the resolution cell, which includes a greater effective number N_s of scatterers; the central limit theorem applies, and the \mathcal{K} -distribution tends to a negative exponential function (statistics follow the Gaussian complex model or the Rayleigh distribution in amplitude). Moreover, in this angular sector, the slope of the shape parameter is less for rough seafloors. If the seabed has a very rough interface, the number of scatterers is strongly variable, and the shape parameter tends to low values.

A particular angle splitting the last two sectors is defined as the point where slopes of shape-parameter curves reverse for soft sediments. Rough seafloors do not seem to exhibit this transition angle. This inversion is explained by the combined effects of the random character of incidence angles and the angular dependence of the backscattering strength. Soft sediment's acoustical responses show a slope change at grazing angles, on the opposite side from sites 1 and 6 showing almost flat backscattering strength angular evolution, which is characteristic of rough seabeds.

Both parameters of the \mathcal{K} -distribution for sidescan sonar data are displayed according to the incidence angle in Figs. 8 and 9. As mentioned previously, due to erroneous recording settings, the shape-parameter values of both sonar systems cannot be quantitatively compared. Nevertheless, a qualitative analysis shows that the split according to angular sectors (specular/intermediate/grazing) is globally preserved. Separation, according to the bottom roughness, is clearly verified. Moreover, Fig. 9 shows an inversion of the shape-parameter evolution slope beyond $\pm 75^\circ$. Shallower incidences are necessary to observe this effect for rough seafloors. This analysis shows that the shape parameter is a discriminating descriptor

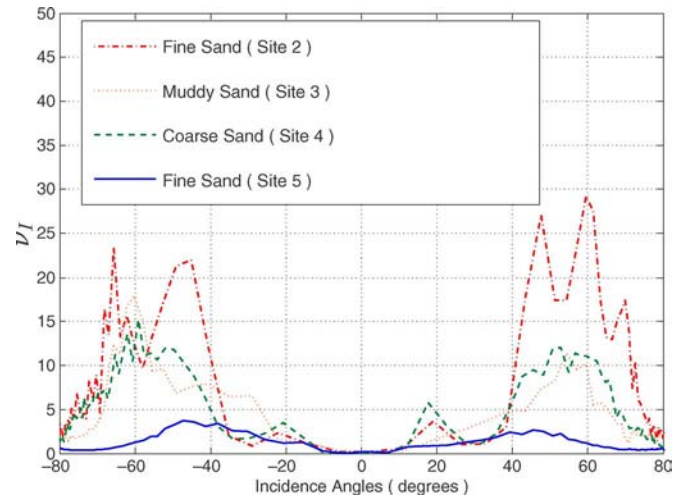


Fig. 8. Angular evolution of the shape parameter ν_I for sidescan sonar data and soft sediments.

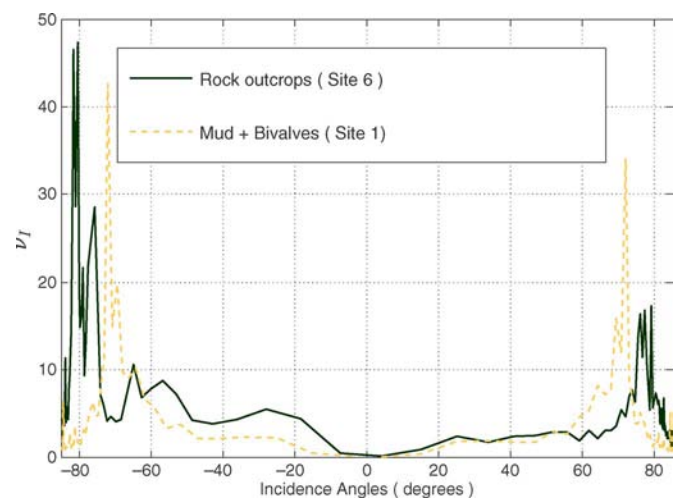


Fig. 9. Angular evolution of the shape parameter ν_I for sidescan sonar data and rough sediments.

of seafloors. Both systems with different characteristics obtain identical angular evolution. In the next section, our approach is compared to other available models in order to fit the shape-parameter evolution.

D. Fitting of the Shape-Parameter Angular Evolution

In this section, experimental measurements of the shape-parameter angular evolution are fitted with OMs, ADKs, and the present improved model (EADK). Fits are compared on six seafloor configurations to determine the capability to model various interface conditions.

The optimization has consisted in solving the nonlinear least square problem and has been resolved with the standard MATLAB function `lsqnonlin`. This algorithm is a subspace trust region method and is based on the interior reflective Newton method.

As a preliminary, backscattering measurements are fitted with ADK (14) and EADK (16). In order to quantify differences, the square root of the mean-squared differences (rms)

TABLE II
FITTING RESULTS OF THE BACKSCATTERING STRENGTH FOR THE ADK MODEL (A AND B ARE EXPRESSED IN DECIBELS)

Site	ADK Model				
	RMS	A	α	B	β
Mud+Bivalves (1)	2.89	2.8	351	-24.1	2
Fine Sand (2)	1.34	-14.4	362	-34.8	2
Muddy Sand (3)	1.60	-13.9	311	-31.4	2
Coarse Sand (4)	1.40	-3.9	547	-19.8	2
Fine Sand (5)	1.12	-13.3	370	-34.8	2
Rock Outcrops (6)	2.30	-11.6	463	-19.3	2

TABLE III
FITTING RESULTS OF THE BACKSCATTERING STRENGTH FOR THE EADK MODEL (A AND B ARE EXPRESSED IN DECIBELS)

Site	EADK Model				
	RMS	A	α	B	β
Mud+Bivalves (1)	0.70	1.93	319	-28.6	0.43
Fine Sand (2)	1.22	-14.2	387	-33.8	2.31
Muddy Sand (3)	1.21	-14.0	296	-33.2	1.41
Coarse Sand (4)	0.75	-3.8	508	-21.8	1.30
Fine Sand (5)	0.95	-13.0	400	-33.8	2.33
Rock Outcrops(6)	0.64	-11.0	338	-23.2	0.78

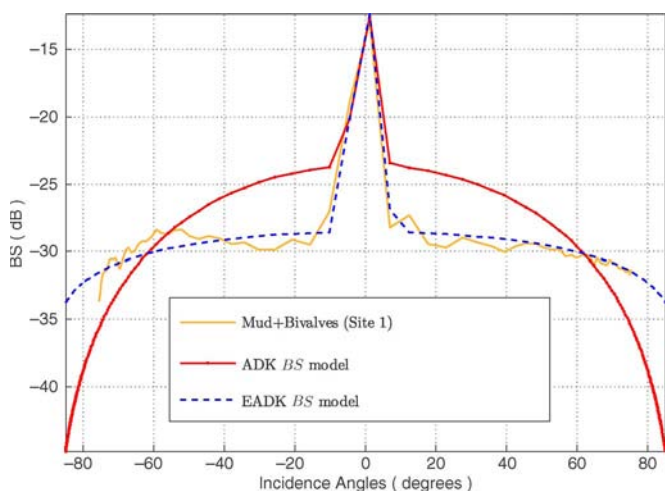


Fig. 10. Backscattering strength measurements for the Mud+Bivalves (Site 1) seafloor, plotted with both ADK and EADK backscattering strength models.

between measurements and fitted model values is computed for each seafloor and is reported in Tables II and III with model input parameters. Figs. 10–15 displays measurements with both fitted models.

The use of the more realistic backscattering strength model as introduced in the EADK model is particularly relevant when observing a variety of seafloors. Results (Tables II and III) show the superiority of the EADK backscattering strength model. In particular, the ADK model cannot correctly model rough-seafloor backscattering strength measurements (Figs. 10 and 15). In addition, soft-seafloor backscattering strength measurements (Figs. 11 and 14) are not accurately fitted for intermediate angles ($[\pm 15^\circ - 50^\circ]$) neither by the EADK model nor by the ADK model. The constant decreasing slope of backscattering strength measurements could be modeled more precisely by adding a transitory component (Gaussian) linking the specular sector and the grazing-angle sector [22].

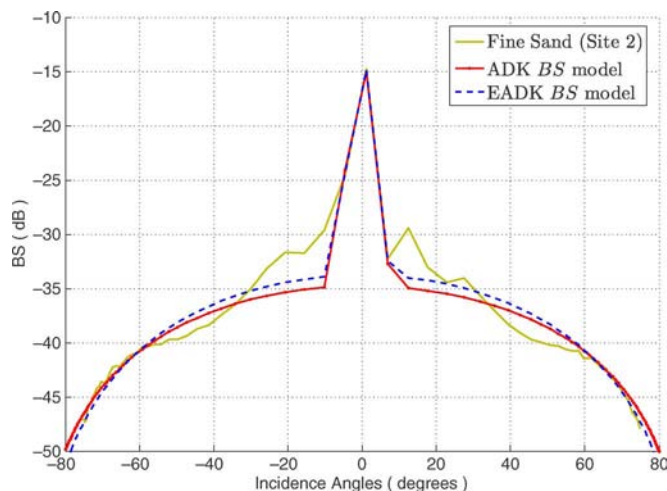


Fig. 11. Backscattering strength measurements for the Fine-Sand (Site 2) seafloor, plotted with both ADK and EADK backscattering strength models.

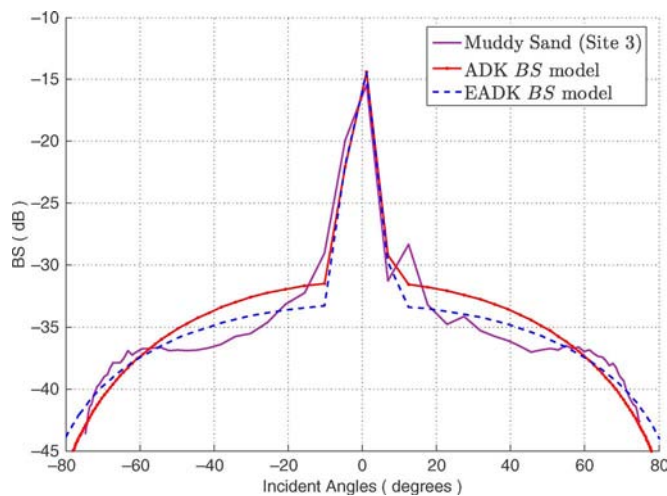


Fig. 12. Backscattering strength measurements for the Muddy-Sand (Site 3) seafloor, plotted with both ADK and EADK backscattering strength models.

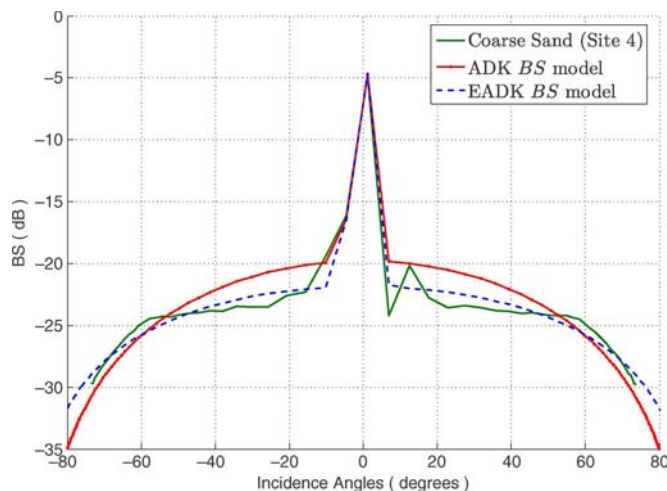


Fig. 13. Backscattering strength measurements for the Coarse-Sand (Site 4) seafloor, plotted with both ADK and EADK backscattering strength models.

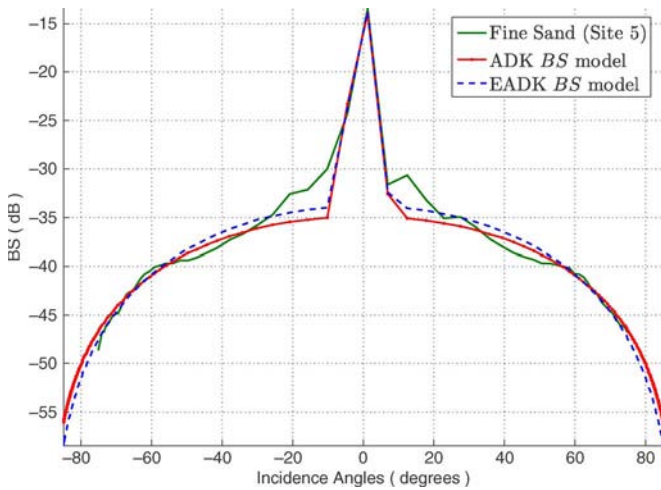


Fig. 14. Backscattering strength measurements for the Fine-Sand (Site 5) seafloor, plotted with both ADK and EADK backscattering strength models.

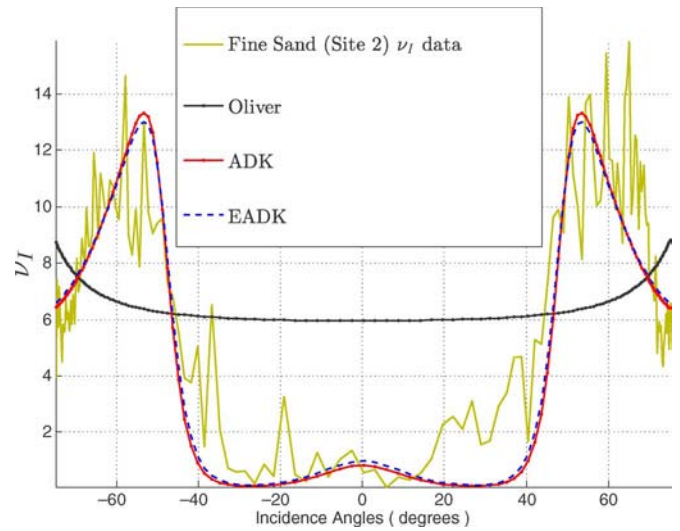


Fig. 17. Shape-parameter ν_I angular evolution for the Fine-Sand (Site 2) seafloor, plotted with three theoretical models (OM, ADK, and EADK).

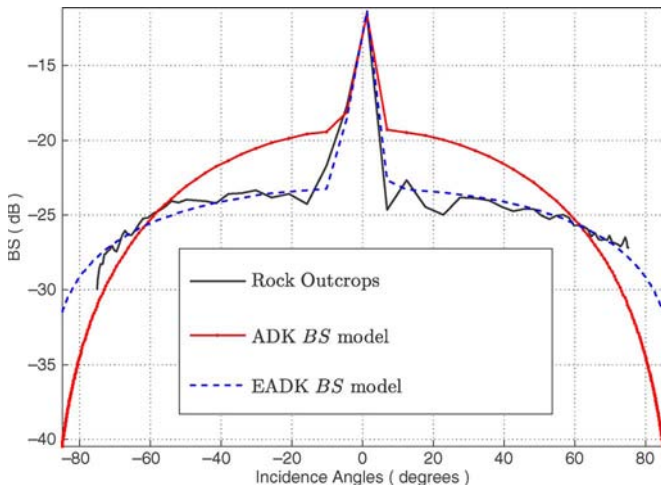


Fig. 15. Backscattering strength measurements for the Rock-Outcrops (Site 6) seafloor, plotted with both ADK and EADK backscattering strength models.

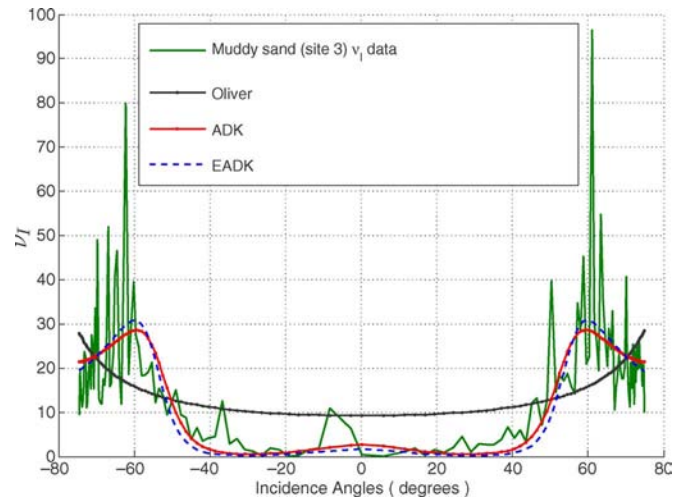


Fig. 18. Shape-parameter ν_I angular evolution for the Muddy-Sand (Site 3) seafloor, plotted with three theoretical models (OM, ADK, and EADK).

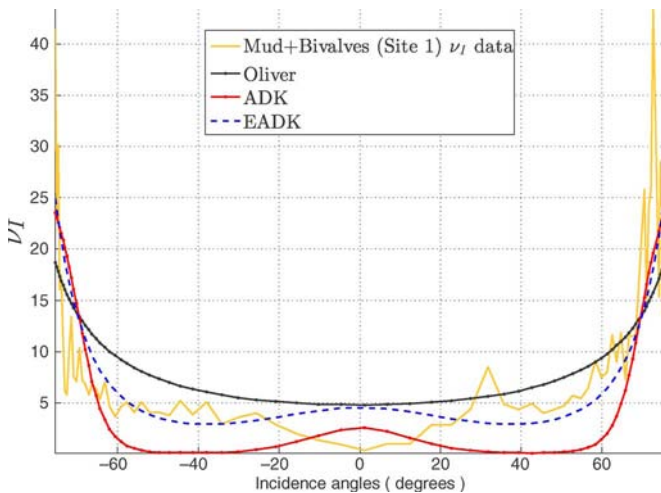


Fig. 16. Shape-parameter ν_I angular evolution for the Mud+Bivalves (Site 1) seafloor, plotted with three theoretical models (OM, ADK, and EADK).

The second and final step of this paper consists of fitting the shape-parameter ν_I angular evolution with the three available models (OM, ADK, and EADK). Figs. 16–21 display results for each sedimentary site. The rms indexes are computed and are summarized in Tables IV–VI with input model parameters.

First, OM is limited in its capability to model the shape-parameter angular evolution. This model is unable to provide the angular evolution. In particular, it cannot explain the characteristic inversion of the slope observed for soft sediments (Figs. 17–20). With the introduction of an intensity angular variation, ADK and EADK models undeniably improve Oliver’s results over the whole data set (Tables IV–VI). The comparison of ADK and EADK models brings the following observations.

- 1) For specular angles ($[-20^\circ, 20^\circ]$), the models do not fit the data. The model validity is to be discussed further for this angular sector.
- 2) Both models show identical evolution (Figs. 17–20) and rms indexes (Tables IV–VI) for both fine-sand seafloors (sites 2 and 5). Previously, backscattering strength

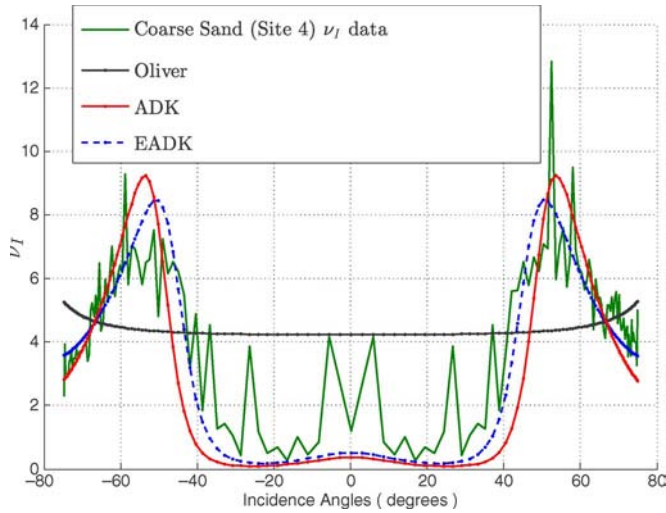


Fig. 19. Shape-parameter ν_I angular evolution for the Coarse-Sand (Site 4) seafloor, plotted with three theoretical models (OM, ADK, and EADK).

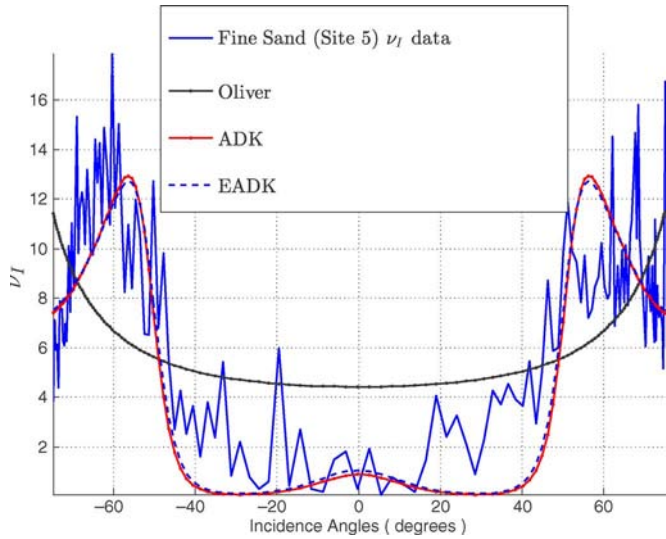


Fig. 20. Shape-parameter ν_I angular evolution for the Fine-Sand (Site 5) seafloor, plotted with three theoretical models (OM, ADK, and EADK).

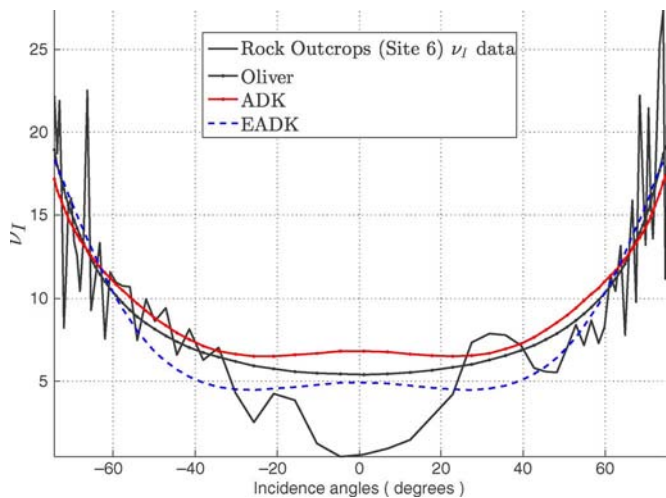


Fig. 21. Shape-parameter ν_I angular evolution for the Rock-Outcrops (Site 6) seafloor, plotted with three theoretical models (OM, ADK, and EADK).

TABLE IV
RESULTS FITTING OF THE ν_I SHAPE-PARAMETER ANGULAR EVOLUTION FOR OM

Site	Oliver Model			RMS
	Lc_t	Lc_l	ν_R	
Mud+Bivalves (1)	5.0	0.03	0.44	6.3
Fine Sand (2)	2.7	2.89	5.71	3.8
Muddy Sand (3)	3.8	0.53	5.43	13.4
Coarse Sand (4)	4.9	5.00	4.14	1.9
Fine Sand (5)	1.0	1.04	3.40	3.6
Rock Outcrops(6)	5.0	0.12	1.25	3.3

TABLE V
RESULTS FITTING OF THE ν_I SHAPE-PARAMETER ANGULAR EVOLUTION FOR THE ADK MODEL

Site	ADK Model			RMS
	Lc_t	Lc_l	σ	
Mud+Bivalves (1)	0.26	0.04	13.04	6.34
Fine Sand (2)	1.50	0.54	10.21	2.10
Muddy Sand (3)	1.18	0.11	12.16	10.64
Coarse Sand (4)	0.71	1.16	10.91	1.42
Fine Sand (5)	8.56	0.45	10.61	2.80
Rock Outcrops(6)	2.16	0.07	21.74	3.71

TABLE VI
RESULTS OF THE FIT OF THE ν_I SHAPE-PARAMETER ANGULAR EVOLUTION FOR THE EADK MODEL

Site	EADK Model			RMS
	Lc_t	Lc_l	σ	
Mud+Bivalves (1)	9.99	0.01	20.88	5.58
Fine Sand (2)	1.79	0.41	10.38	2.04
Muddy Sand (3)	1.79	0.19	11.86	10.52
Coarse Sand (4)	9.90	0.82	11.07	1.80
Fine Sand (5)	1.47	0.34	10.74	2.73
Rock Outcrops(6)	1.81	0.05	22.53	3.38

angular measurements were fitted with an EADK model input parameter β close to two (Table III). For these seafloors, ADK and EADK models are obviously equivalent. As expected, the series expansion approximating the analytical solution for the EADK model did not generate prohibitive errors. Moreover, fits are very accurate at grazing angles.

- 3) The EADK model for other soft-seafloor (Figs. 18 and 19) match with the data more accurately than the ADK model.
- 4) Fits on rough seafloors (Figs. 16 and 21) are definitely better for the EADK model. For these seafloor configurations, the backscattering strength angular behavior clearly differs from the Lambert law (Table III). This makes clear the importance of the backscattering strength model and justifies the use of the EADK model.

The quantitative interpretation of the EADK model input parameters is not straightforward. However, the σ standard-deviation values obtained from fitting (Table VI) show an interesting trend according to the seafloor. The values for rough seafloors (Rocks and Mud+Bivalves) are much higher (around 20°) compared to other seafloor configurations. Moreover, the rougher the sediment, the less Lc_l . In other words, the correlation of individual scatterer amplitudes is very low which seems consistent with the definition of heterogeneity. Lastly, the practical use of these models highlights the fact that the Lc_t cross-track correlation-length variations have little

consequence on the simulated shape-parameter values. The extent of the resolution cell in the along-track direction is much larger than the one in the across-track direction and is responsible for the difference of both input-parameter influence [17].

Fitting specular angle measurements is not accurate. Physical models of backscattering strength are also based on a splitting into angular sectors [23]. At specular angles, models are based on the effect of “facets” oriented perpendicularly to the incident sound wave direction. At low grazing angles, laws of the geometrical diffusion apply and the small perturbation theory is used; backscattering is controlled by the effects due to the microrelief.

An adaptation of this approach to the statistical models can be carried out. If the small perturbation model is used at grazing angles, it implies that surface roughness dominates the physical process and interference phenomena appear within the resolution cell. The scatterer model, key point of Oliver’s work, is then valid.

For specular angles, the existence of oriented facets assumes that a small set of scatterers dominates the process, invalidating the scatterers’ model hypotheses. This may explain why fitting the shape-parameter model is not successful in this angular sector.

IV. CONCLUSION

In this paper, an improved model of backscattering statistics is proposed. It advantageously takes into account sonar system characteristics (array geometry and signal duration) and seafloor properties (backscattering strength and statistical description of the interface). Data from two high-resolution sonar systems (multibeam echosounder and sidescan sonar) have been analyzed. Since the \mathcal{K} -distribution has previously shown a good capacity and robustness to model each of these measurements, a study of the \mathcal{K} -parameter’s angular evolution was carried out. Both parameters (one is energetic and the other is linked to the seafloor-surface roughness) show typical angular behaviors discriminating the seafloor for both sonar systems. The proposed model is validated on measurements from six seafloor configurations and shows significant improvement when compared with two other previous models.

APPENDIX

PROCESSING OF DF1000 SIDESCAN SONAR DATA FOR SEAFLOOR CHARACTERIZATION

In order to retrieve the backscattering strength of a target, sonar data have to be compensated according to the sonar (24). In the particular case of seafloor-mapping sonars, the angular response has to be estimated from a time-dependent recorded-echo signal. For sidescan sonar data, this method encompasses two phases: accurate computation of the relation between the time of recorded samples and the incidence angle of reception and assessment of the energetic conversion factors of the acoustical wave. The intensity balance is given by the sonar equation (here expressed in decibels)

$$BS(\theta) = RE - EL + 2TL(\theta) - 10 \log_{10}(IA(\theta)) - SH - PG - AP(\theta) \quad (24)$$

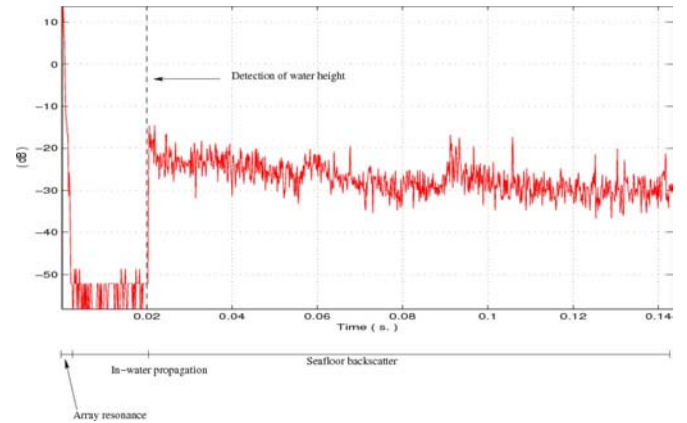


Fig. 22. Echo level recorded by the sidescan sonar.

where $BS(\theta)$ is the backscattering strength, RE is the received echo recorded by the sonar, EL is the emitted level, $TL(\theta)$ is the in-water transmission losses (absorption due to the seawater and loss of energy due to the spherical nature of the acoustical wave), $IA(\theta)$ is the insonified area (the footprint) of the signal on the seafloor, SH is the sensibility of array in reception, PG is the processing gain (amplification of the signal and TVG law), and $AP(\theta)$ is the array pattern.

In the particular case of our DF1000 sonar, for each 0.1-ms emitted signal, the seafloor echo level (RE) is recorded during approximately 140 ms (Fig. 22). For each echo, the signal is characterized by a quick decrease at the end of the emitted signal (resonance of the array), a low-level plateau due to the wave propagation in the water and, finally, the seafloor response.

For each signal, the height between the sonar tow fish and the seafloor is first estimated with a threshold detection of the seafloor specular echo (Fig. 22). Emitted angles are then obtained from this estimated height (assuming a locally flat seafloor) together with roll and pitch information (the two last were simultaneously recorded by the sonar system). Emitted angles are finally corrected from seafloor local slope in order to obtain the actual incidence angles onto the sediment: a digital terrain model was computed from the EM1000 bathymetric data.

In a second step, the received acoustical signal level is used to estimate the backscattering strength. The TVG law, amplification factor, and the emitted level were first used as provided by the manufacturer. A series of calibration measurements had to be performed in the IFREMER test tank, leading to more accurate knowledge of the sonar parameters: the emitted signal, the array sensitivity, and across- and along-track array patterns (Fig. 23). These measured values were finally introduced for inversion of (24). Concerning the transmission losses, the seawater absorption-coefficient values were estimated from *in situ* temperature measurements.

Although this method made it possible to retrieve backscattering strength values from sidescan sonar data, the quality of the results cannot compare with those from a multibeam echosounder. The reason for this is the difficulty to establish accurate relations between time and incident angle without a measurement of bathymetry; another problem is met close to

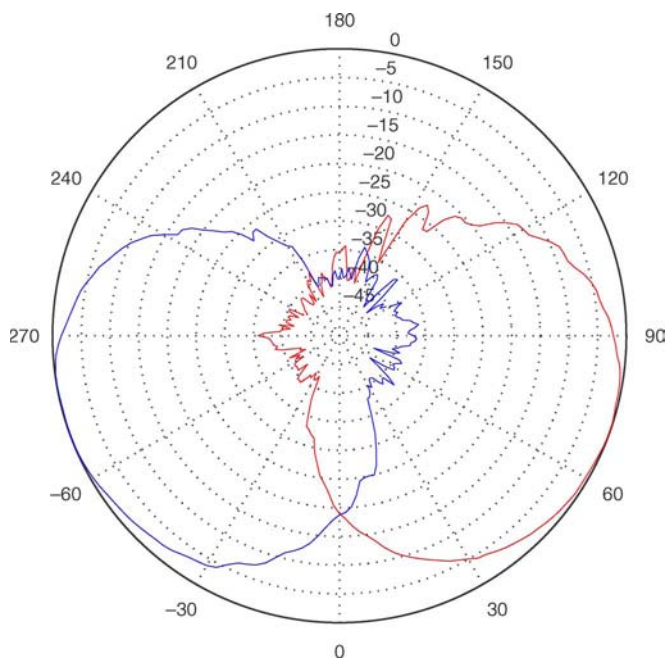


Fig. 23. Across-track array patterns of the sidescan sonar.

nadir, where the array sensitivity collapses and phenomena linked to crosstalk are likely to occur while at the same time the time-angle relation becomes specially unstable.

REFERENCES

[1] E. Jakeman *et al.*, "Significance of K distributions in scattering elements," *Phys. Rev. Lett.*, vol. 40, no. 9, pp. 546–550, Feb. 1978.
 [2] M. Gensane, "A statistical study of acoustic signals backscattered from the sea bottom," *IEEE J. Ocean. Eng.*, vol. 14, no. 1, pp. 84–93, Jan. 1989.
 [3] S. Stanic and E. Kennedy, "Fluctuations of high-frequency shallow-water sea-floor reverberation," *J. Acoust. Soc. Amer.*, vol. 91, no. 4, pp. 1967–1973, Apr. 1992.
 [4] W. Stewart *et al.*, "Quantitative sea-floor characterization using a bathymetric sidescan sonar," *IEEE J. Ocean. Eng.*, vol. 19, no. 4, pp. 599–610, Oct. 1994.
 [5] A. Lyons and D. Abraham, "Statistical characterization of high-frequency shallow-water sea-floor backscatter," *J. Acoust. Soc. Amer.*, vol. 106, no. 3, pp. 1307–1315, Sep. 1999.
 [6] A. Lyons, W. Fox, T. Hasiotis, and E. Pouliquen, "Characterization of the two-dimensional roughness of wave-rippled sea floors using digital photogrammetry," *IEEE J. Ocean. Eng.*, vol. 27, no. 3, pp. 515–524, Jul. 2002.
 [7] P. Crowther, *Fluctuation Statistics of Sea-Bed Acoustic Backscatter*. New York: Plenum, 1980, pp. 609–622.
 [8] D. Middleton, "New physical-statistical methods and models for clutter and reverberation: The KA-distribution and related probability structures," *IEEE J. Ocean. Eng.*, vol. 24, no. 3, pp. 261–284, Jul. 1999.
 [9] S. MacDaniel, "Seafloor reverberation fluctuations," *J. Acoust. Soc. Amer.*, vol. 88, no. 3, pp. 1530–1535, Sep. 1990.
 [10] D. Abraham and A. Lyons, "Novel physical interpretations of K -distributed reverberation," *IEEE J. Ocean. Eng.*, vol. 27, no. 4, pp. 800–813, Oct. 2002.
 [11] C. Oliver, "A model for non-Rayleigh scattering statistics," *Opt. Acta*, vol. 31, no. 6, pp. 701–722, 1984.
 [12] L. Hellequin, J. Boucher, and X. Lurton, "Processing of high frequency multibeam echosounder data for seafloor characterization," *IEEE J. Ocean. Eng.*, vol. 28, no. 1, pp. 78–89, Jan. 2003.
 [13] E. Jakeman *et al.*, "Generalized K distribution in scattering experiments," *J. Opt. Soc. Amer. A, Opt. Image Sci.*, vol. 4, no. 9, pp. 1764–1772, 1987.
 [14] C. Oliver and S. Quegan, *Synthetic Aperture Radar Images*. Norwood, MA: Artech House, 1998.
 [15] E. Jakeman, "Non Gaussian models for the statistics of scattered waves," *Adv. Phys.*, vol. 37, no. 5, pp. 471–529, 1988.

[16] C. Oliver, "Correlated K -distributed clutter models," *Opt. Acta*, vol. 32, no. 12, pp. 1515–1547, 1985.
 [17] G. Le Chenadec, "Analyse de descripteurs énergétiques et statistiques pour la caractérisation des fonds marins," Ph.D. dissertation, Univ. de Bretagne Occidentale, Brest, France, 2004.
 [18] J. Augustin and X. Lurton, "Image amplitude calibration and processing for seafloor mapping sonars," in *Proc. IEEE Oceans—Europe*, 2005, vol. 1, pp. 698–701.
 [19] F. Wilcoxon, "Individual comparisons by ranking methods," *Biometrics*, vol. 1, no. 6, pp. 80–83, Dec. 1945.
 [20] M. Fisz, *Probability Theory and Mathematical Statistics*. Hoboken, NJ: Wiley, 1963.
 [21] C. Oliver, "Optimum texture estimators for SAR clutter," *J. Phys. D, Appl. Phys.*, vol. 26, no. 11, pp. 1824–1835, 1994.
 [22] X. Lurton, *An Introduction to Underwater Acoustics: Principles and Applications*. New York: Springer-Verlag, 2002.
 [23] H. Medwin and C. Clay, *Fundamentals of Acoustical Oceanography*. New York: Academic, 1998.



Gilles Le Chenadec was born in 1974. He received the M.Sc. degree in applied acoustics from the Université du Maine, Le Mans, France, and the Ph.D. degree from the Université de Bretagne Occidentale, Brest, France. The subject of his Ph.D. focuses on seafloor characterization from sonar data.

While completing his doctoral work, he worked with both the École Nationale Supérieure des Télécommunications, France and IFREMER, Plouzane, France. In 2005–2006, during a postdoctoral period conducted at the France Telecom R&D, he focused

on issues regarding detection and characterization of human expressions of emotions. His research interests include subjects related to signal processing and analysis and machine learning.



Jean-Marc Boucher (M'83) was born in 1952. He received the engineering degree in telecommunications from the École Nationale Supérieure des Télécommunications, Paris, France, and the Habilitation à Diriger des Recherches degree from the University of Rennes 1, Rennes, France, in 1975 and 1995, respectively.

He is currently a Professor with the Department of Signal and Communications, École Nationale Supérieure des Télécommunications de Bretagne, France. His research interests include estimation theory and classification, Markov models, blind deconvolution, wavelets, and multiscale image analysis, with applications to radar and sonar, seismic, and biological signals. He has published approximately 100 papers in these areas in international journals and conferences.

and classification, Markov models, blind deconvolution, wavelets, and multiscale image analysis, with applications to radar and sonar, seismic, and biological signals. He has published approximately 100 papers in these areas in international journals and conferences.



Xavier Lurton was born in Bordeaux, France, in 1955. He received the Ph.D. degree in applied acoustics from the Université du Maine, Le Mans, France, in 1979.

From 1981 to 1989, he was with Thomson-Sintra ASM, working in the field of underwater sound propagation modeling for naval applications. In 1989, he joined IFREMER, Plouzane, France, the French oceanological research agency. After working on various acoustical oceanography applications (ocean tomography, telemetry, and fisheries sonar) and managing the IFREMER acoustics laboratory for five years, he is now in charge of a research program on seafloor characterization using multibeam echosounders. His current interests are both in the physics of seabed backscattering and in sonar engineering and signal processing.

managing the IFREMER acoustics laboratory for five years, he is now in charge of a research program on seafloor characterization using multibeam echosounders. His current interests are both in the physics of seabed backscattering and in sonar engineering and signal processing.